

# Pushing Photons with Electrons: Observation of the Polariton Drag Effect

D. M. Myers,<sup>\*</sup> Q. Yao, S. Mukherjee,<sup>†</sup> B. Ozden,<sup>‡</sup> J. Beaumariage, and D. W. Snoke  
*Department of Physics and Astronomy, University of Pittsburgh, Pittsburgh, PA 15260, USA*

L. N. Pfeiffer and K. West  
*Department of Electrical Engineering, Princeton University, Princeton, NJ 08544, USA*  
(Dated: July 8, 2022)

We show the direct effect of free electrons colliding with polaritons, changing their momentum. The result of this interaction of the electrons with the polaritons is a change in the angle of emission of the photons from our cavity structure. Because the experiment is a photon-in, photon-out system, this is equivalent to optical beam steering of photons using a DC electrical current. The effect is asymmetric, significantly slowing down the polaritons when they move oppositely to the electrons, while the polaritons are only slightly accelerated by electrons moving in the same direction. We present a theoretical model which describes this effect as well as energy dissipation in a polariton condensate.

It has long been known that an electron can impart momentum to an exciton-polariton through the scattering interaction with the exciton part of the polariton. Apart from the intrinsic interest in demonstrating this effect, it may have application in steering the direction of light emission by a DC electrical current, with the angle of deflection directly controlled by the applied current. However, observation of this effect has remained elusive. In this Letter we report observation of this effect with exciton-polaritons in a solid-state microcavity.

The physics of exciton-polaritons has been widely explored in recent years, and is well summarized in recent reviews, many of which have focused on Bose-Einstein condensation of polaritons [1–4]. In the present work, we use a polariton condensate, but the effect is not fundamentally one that only occurs for a condensate; rather, the condensate produces a spectrally narrow emission over a wide area that makes the polariton drag effect easy to observe. Superfluidity of the condensate does not prevent the drag effect, because it is equivalent to a body force, or longitudinal force. The structures we use also allow long-distance transport over hundreds of microns [5, 6], which allows good momentum resolution in our measurements.

Recent theoretical work taking into account the polaron effect on an exciton interacting with a Fermi sea [7] has predicted that applied DC current will give a drag force on exciton-polarons, and that the effect will also be significant when the excitons are coupled to photons, as in an exciton-polariton system [8]. However, the drag effect can be understood even apart from the polaron effect as a purely collisional exchange of momentum due to Coulombic collisions between electrons and the excitonic part of a polariton, as discussed, e.g., in Ref. 9 and references therein. Other work [10–12] envisioned a drag effect between separated layers of excitons and free electrons, but this is not crucial for the effect, as free electrons can also move in the same quantum wells as the excitons.

**Experiment.** Exciton-polaritons in the strong-coupling limit were made by placing semiconductor quantum wells at the antinodes of a planar optical cavity. These semiconductor layers have excitons nearly resonant in energy with a cavity photon mode. If the  $Q$ -factor of the cavity is high enough, and the coupling of the photon and exciton states is strong enough, new eigenstates appear which are no longer purely photon or exciton, but a superposition of both. In other words, a photon in the cavity spends some fraction of its time as an excited electron-hole pair.

The sample used in this experiment consists of a  $3\lambda/2$  microcavity formed by two distributed Bragg reflectors (DBRs), grown by molecular beam epitaxy (MBE). The DBRs were both made of alternating layers of  $\text{Al}_{0.2}\text{Ga}_{0.8}\text{As}$  and  $\text{AlAs}$ , with 32 periods in the top DBR and 40 in the bottom. 4 quantum wells (QWS), made of 7 nm GaAs layers with AlAs barriers, were placed at each of the 3 antinodes of the cavity. This microcavity design is the same used in previous work [5, 6, 13–17]. Long wires ( $\approx 200 \mu\text{m} \times 20 \mu\text{m}$ ) were formed by etching away the top DBR, confining the polaritons within the wire and exposing the QWs.

To allow co-linear motion of free electrons in the same medium, two NiAuGe contacts were then placed upon the QWs at the ends of the wire, allowing electrical injection into the QWs (see Figure 1). Hall measurements show that the wire regions are intrinsically  $n$ -doped of the order of  $10^{13} \text{ cm}^{-3}$ , and the contacts are  $n$ -type with heavy doping of the order of  $10^{19} \text{ cm}^{-3}$ . A continuous-wave (cw) stabilized M Squared Ti:sapphire pump laser was used to excite a spot on the wire, with a spot size of about  $20 \mu\text{m}$  FWHM, in the same arrangement used in Ref. 17. The pump was non-resonant, with an excess energy of about 100 meV, and mechanically chopped at 400 Hz with a pulse width of about 60  $\mu\text{s}$ . A source meter was used to sweep the applied voltage along the wires while measuring electrical current. The details of the fabrication and the electrical measurement are dis-

cussed in Ref. 16. The wire devices used in this study were all near resonance between the cavity and exciton modes ( $\delta = E_{\text{cav}} - E_{\text{exc}} = 0$ ).

Off-resonant optical pumping of this type of structure produces a cloud of excitons, which then lose energy and fall down into polariton states. As in previous experiments with similar structures [14, 17], there are two density thresholds for the optical excitation. At the lower threshold, a local quasicondensate is formed at the excitation spot, which can then ballistically expand away from the excitation region; above a higher critical threshold, the condensate jumps down dramatically into a much lower energy state, which is spectrally very narrow ( $< 0.1$  meV width at half maximum), has high coherence length ( $\gg 200 \mu\text{m}$ ), and fills most of the available space in a potential-energy minimum. We define the pump power needed to reach this second threshold as  $P_{\text{thres}}$ . The condensate was observed by recording the photons that leak out of the top mirror, using conventional imaging optics for both real-space (near field) and momentum-space (far field, Fourier plane) images, and a spectrometer for energy resolution. The leakage of photons out of the cavity was a tiny fraction of the population at any moment in time, because the  $Q$  of the cavity is very high ( $\sim 350,000$ ), so that a steady-state population was maintained. In this steady state, the energy and spatial distribution of the polariton condensate is determined by the external potential profile it feels, which is a combination of the single-particle polariton dispersion and the repulsion of polaritons from slow-moving excitons with much higher mass, and the density-dependent, repulsive polariton-polariton interaction, which tends to flatten any external potential felt by the polaritons.

**Experimental Results.** The experimental arrangement is shown in Figure 1, which gives the definitions of the axes directions and shows the voltage connections. Unless otherwise specified, the pump spot was located near the left ( $x = 0$ ) end of the wire for all of the data shown in this work. Figure 2 shows the polariton distribution along the wire at two different pump powers above threshold and at zero applied voltage. The energy “hill” near  $40 \mu\text{m}$  is due to the large population of excitons at the pump spot, which repulsively interact with the polaritons. The dips at the ends of the wire are due to the increased strain from the etching, similar to the corners of the square pillars discussed in Ref. 14. A shallow cavity gradient along the  $+x$ -direction caused a small slope in the potential, with a total energy drop of about  $0.5$  meV across the wire. At the lower power, a quasi-condensate at the location of the pump is clearly visible at high energy, as well as a significant population in the left-side end trap and a smaller population in the right-side trap. In the level region on the side away from the pump, a large mono-energetic condensate forms, filling a region of the wire about  $100 \mu\text{m}$  long. At higher power, the population on the right becomes large enough

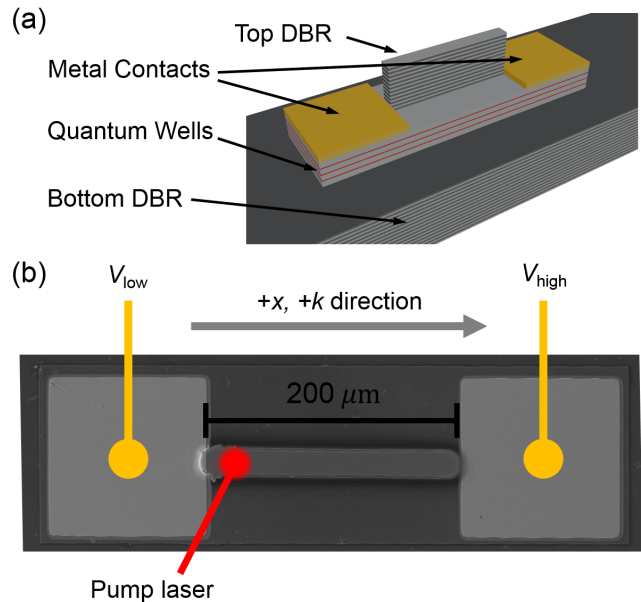


FIG. 1. a) The etched microcavity structure with the NiAuGe contacts at each end of the wire. (b) Scanning electron microscope (SEM) image of a representative etched wire, with an overlay showing the experimental arrangement. The voltage connections of the source were connected to the device as shown. Thus, positive conventional current flowed in the direction of  $-x$ .

to have repulsive interactions that shift it up in energy, forming a single, nearly mono-energetic condensate.

Figure 3 shows the energy and in-plane momentum ( $k_{\parallel}$ ) distribution of the polaritons at two different applied voltages. A population near  $k_{\parallel} = 0$  and at slightly lower energy is visible, and is emitted from the end of the trap. The larger population is from the level region of the wire, and clearly has an overall nonzero in-plane momentum, even with zero applied voltage. This is due to flow in the main part of the wire, away from the pump spot, in the  $+x$ -direction. With applied negative voltage (Figure 3(b)), while all the other experimental conditions remain the same, the overall momentum is clearly reduced. This voltage corresponds to conventional current flowing in the  $+x$ -direction, and thus electron current flowing in the  $-x$ -direction, which opposes the polariton flow. This clearly shows an effect of drag upon the polaritons from the electrical current. When the wire is pumped on the other end, the overall effect is reversed, with the polaritons moving with momentum in the opposite direction. However, because the gradient of the cavity is in the opposite direction relative to the flow away from the pump in that case, the overall drag effect is reduced (see the Supplemental Information for further data and discussion).

Figure 4 shows the polariton distribution vs.  $k_{\parallel}$  for multiple applied voltages. A clear shift in the momen-

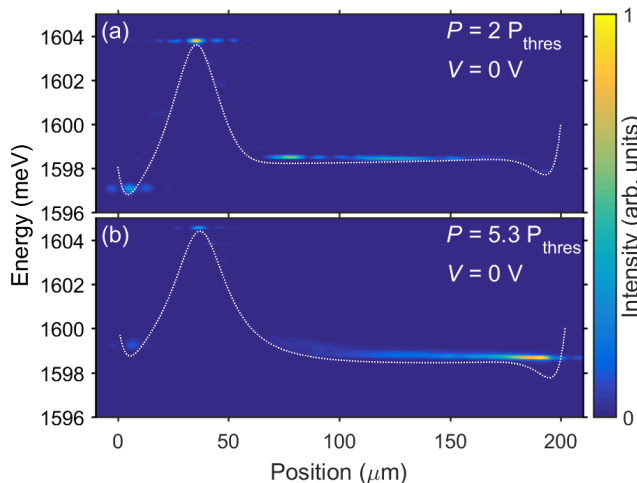


FIG. 2. PL intensity vs. energy and position along the length of the wire at zero applied voltage. The white dotted lines give the outline of the potential felt by the polaritons. The threshold power ( $P_{\text{thres}}$ ) was about 114 mW, and the powers used were (a)  $2P_{\text{thres}}$  and (b)  $5.3P_{\text{thres}}$ . The PL intensity was normalized separately for each image.

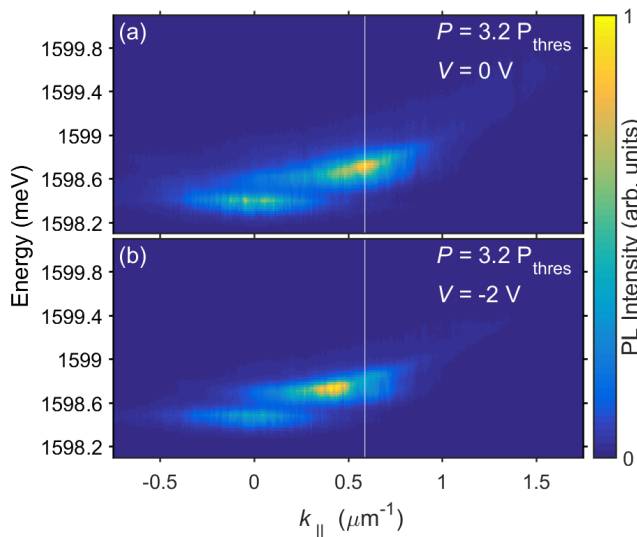


FIG. 3. PL intensity vs. energy and in-plane momentum ( $k_{\parallel}$ ). The threshold power ( $P_{\text{thres}}$ ) was about 114 mW, and the powers used were both about  $3.2P_{\text{thres}}$ . The applied voltage in each case (a) 0 V and (b) -2 V. The white vertical line is marking the  $k_{\parallel}$  value of the peak of the distribution at zero applied voltage to aid in comparing the two images. The PL intensity was normalized separately for each image.

tum is observed under applied voltages of opposite polarity. Simple calculations indicate that the velocities of the electrons and polaritons are comparable. The polariton velocity is measured directly from their momentum;  $0.5 \mu\text{m}^{-1}$  corresponds to  $v = \hbar k/m = 6 \times 10^7 \text{ cm/s}$ . The electron velocity can be estimated from the mobility, which our measurements give as approximately

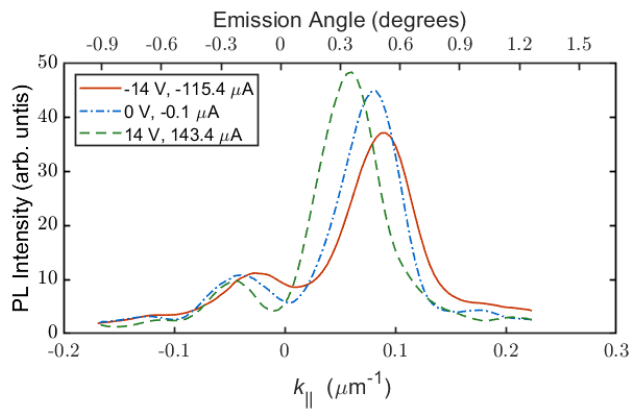


FIG. 4. Time integrated average momentum distribution of the condensate under different applied voltages for the wire shown in Fig. 5. These data are for a wire similar to that used for Figure 3, but with a smaller cavity gradient  $0.0025 \text{ meV}/\mu\text{m}$  and a smaller threshold power of  $P_{\text{thres}} \approx 75 \text{ mW}$ . The power used was  $10.3P_{\text{thres}}$ .

$100 \text{ cm}^2/\text{V}\cdot\text{s}$ . For a voltage drop of 1 V over  $100 \mu\text{m}$ , this gives electron velocities of the order of  $10^6 \text{ cm/s}$ . A blueshift in the chemical potential of the steady-state condensate is also observed in these wires when an electrical current is driven through the wire as shown in Figure 5. The blueshift is greater when the electrons flow opposite to the flow of the condensate and is smaller when the electrons flow co-linear with the condensate.

**Theory.** We have developed a model showing the drag effect originating from the collisions between the electrons and the polaritons in the condensate, based on extending the theory for dissipation in cold atom condensates due to interaction with thermal, non-condensed particles [18–28]. A detailed derivation of this model is given in Ref. [29]. The Gross-Pitaevskii equation describing the polariton condensate ( $\psi$ ) experiencing drag from the electron reservoir in a one-dimensional wire is given by

$$i\hbar\partial_t\psi(x,t) = \left( \frac{1}{2m_\psi}(-i\hbar\partial_x - p_{rel})^2 + V_\psi(x) + U_0|\psi(x,t)|^2 + V_e(x,t) \right) \psi(x,t), \quad (1)$$

where  $m_\psi$  is the mass of the polaritons,  $p_{rel}$  is the relative momentum of the condensate with respect to the electron reservoir,  $U_0$  is the polariton-polariton repulsion, and  $V_\psi(x)$  is the effective potential experienced by the polaritons due to the photonic energy gradient in the microcavity and repulsive potential due to the interaction with the excitons created by the non-resonant pump. The

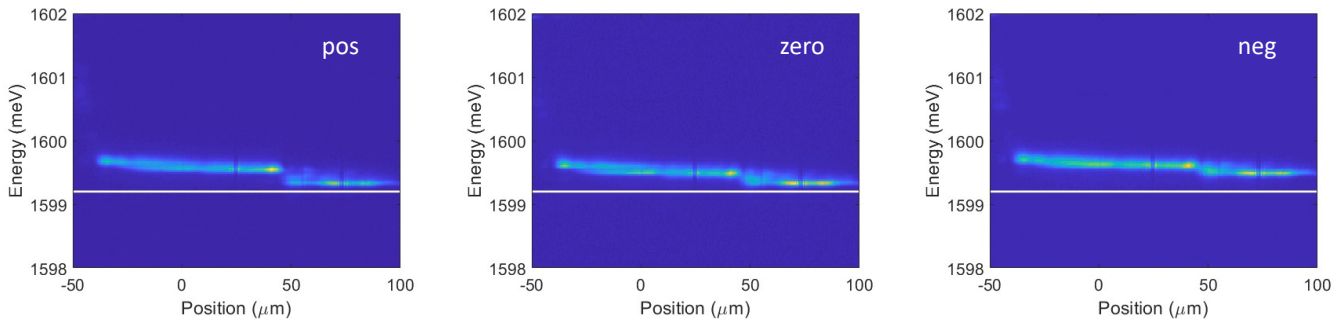


FIG. 5. Time integrated energy spectra of the condensate along the length of the wire at positive (15V), zero, and negative (-15V) voltages. The white lines act as a reference line for observing the relative energy shift under different voltages. In this wire, the threshold power ( $P_{\text{thres}}$ ) was about 75 mW, and the power used was  $10.3P_{\text{thres}}$ . The PL intensity was normalized separately for each image. Time integrated average momentum corresponding to similar conditions is shown in Fig. 4.

field-dependent drag potential is given by

$$V_{\epsilon}(x, t) = - \int dx' M(x - x') \vec{\nabla}' \cdot \underbrace{\left( \frac{\mathbf{p}_{\text{rel}}}{m_{\psi}} |\psi(x')|^2 + \mathbf{j}(x') \right)}_{\mathbf{J}(x')}, \quad (2)$$

where  $M(x - x')$  is the scattering matrix and  $J(x')$  is the polariton condensate current established by the balance between the rate of polariton generation from the CW non-resonant pump  $P(x)$  and the rate of polariton leakage from the cavity  $\gamma$ . The continuity equation describing the rate of change of spatial polariton condensate density  $n(x, t) = |\psi(x, t)|^2$  is given by

$$\frac{dn(x, t)}{dt} = P(x, t) - \gamma n(x, t) - \frac{dJ(x, t)}{dx}. \quad (3)$$

Equations 1 and 3 are time evolved numerically until a steady state solution is found. Details of the numerical simulation is provided in the Supplementary information section.

Time-integrated real-space spectra showing the energy of the condensate are shown in Figure 6, and the time-integrated momentum distribution is shown in Figure 7. These simulations capture the basic effect seen in our experiments; an upward shift of the chemical potential of the condensate which is different depending on the direction of the electron current, and the shift in the average momentum of the polaritons due to drag from the electron reservoir. The drag potential  $V_{\epsilon}(x, t)$  is responsible for energy dissipation of the condensate and is non-zero when a steady state is reached. This is because even in the steady state there is a non-zero spatially inhomogeneous polariton current which is sustained by the decay and generation of the polaritons. Since the condensate is moving to the right, the net momentum is non-zero and positive as shown in the Figure 7 with no applied voltage. When a negative voltage is applied, the moving electrons apply a force on the condensate to the left, which slows down the condensate. Conversely, when a

positive voltage is applied the condensate receives a kick from the moving electron reservoir and the net momentum is increased.

Because the photoluminescence intensity, which directly indicates the density of the condensate, was not found to be significantly different for different applied voltages, we can rule out the shifts in the condensate energy due to the polariton-polariton and polariton-exciton interactions. What remains is the effect of the real-valued effective potential derived for the electron drag in our model, which has the same origin as the drag potential for a cold atom condensate interacting with an incoherent reservoir.

**Conclusions.** We have demonstrated that a DC current can directly alter the momentum of exciton-polaritons; this has the direct effect of changing the angle of photon emission. Since the polaritons are effectively renormalized photons, created by photon absorption and ending with photon emission, this polariton drag is, in effect, using a DC electric current to change the momentum of photons. As polariton structures move ever closer to practical room temperature devices [4], this basic effect may also be possible in those devices.

The theoretical model which describes this effect involves subtle points originally developed for the dissipation and drag of a cold atom condensate interacting with a thermal, incoherent reservoir. Surprisingly, the primary effect of these dissipative interactions is to give a real-valued, density-dependent potential energy term in the Gross-Pitaevskii equation that describes the condensate in steady state. This indicates that it is simplistic to say that condensates do not experience drag or dissipation. In steady state, when there is interaction with an incoherent reservoir of non-condensate particles, they experience both.

**Acknowledgements.** The work at Pittsburgh was funded by the Army Research Office (W911NF-15-1-0466) and by the National Science Foundation (Grant No. DMR-2004570). This research was supported in

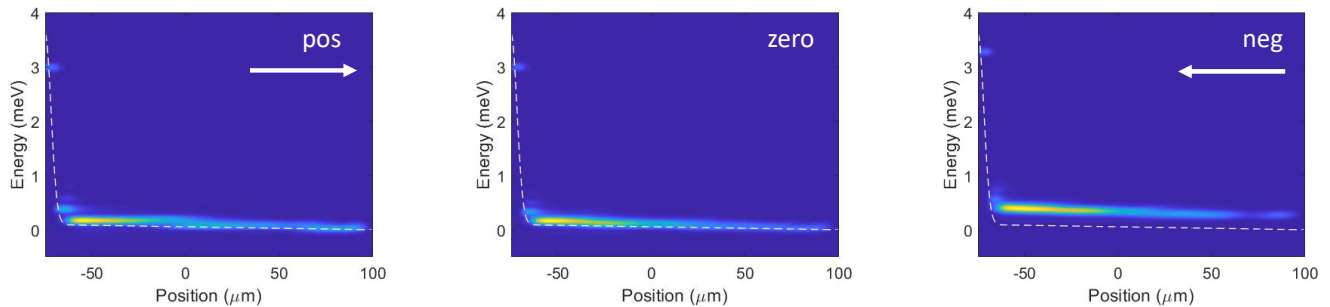


FIG. 6. Theoretical time-integrated spectra of the condensate along the wire for positive, zero and negative velocities of the electron reservoir. Real space spectra obtained by the Fourier transform of the late time wavefunction in a temporal window and integrated over many such windows. The white dashed line outlines the effective potential experienced by the polaritons. In the simulation, the parameters used were  $m_\psi = 1 \times 10^{-4} m_e$ ,  $U_0 = 10 \mu\text{eV}\cdot\mu\text{m}^2$  [30], and the magnitude of the relative velocity is given as  $v_{rel} = 1 \times 10^5$  m/s. Further details on the simulation are provided in the Supplementary information. Each image is plotted on a normalized color scale from 0 - 1.

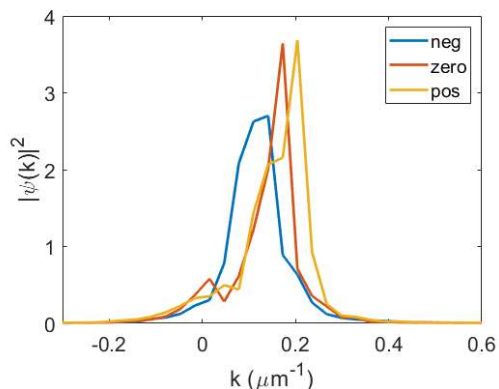


FIG. 7. Time-integrated average momentum of the polaritons in the condensate corresponding to the theory plots in Figure 6.

part by the University of Pittsburgh Center for Research Computing through the resources provided. The work of sample fabrication at Princeton was funded in part by the Gordon and Betty Moore Foundation (GBMF-4420) and by the National Science Foundation MRSEC program through the Princeton Center for Complex Materials (DMR-0819860). We thank Ashton Bradley for helpful conversations.

\* Current address: Kulicke & Soffa Industries Inc., Fort Washington, PA 19034, USA

† smukh.phy@gmail.com

‡ Current address: Department of Physics and Engineering, Penn State Abington, Abington, Pennsylvania 19001, USA

[1] A. V. Kavokin, J. J. Baumberg, G. Malpuech, and F. P. Laussy, *Microcavities*, 2nd ed. (Oxford University Press, 2017).

- [2] I. Carusotto and C. Ciuti, *Rev. Mod. Phys.* **85**, 299 (2013).
- [3] H. Deng, H. Haug, and Y. Yamamoto, *Rev. Mod. Phys.* **82**, 1489 (2010).
- [4] D. W. Snoke and J. Keeling, *Physics Today* **70**, 54 (2017).
- [5] B. Nelsen, G. Liu, M. Steger, D. W. Snoke, R. Balli, K. West, and L. Pfeiffer, *Phys. Rev. X* **3**, 041015 (2013).
- [6] M. Steger, C. Gautham, D. W. Snoke, L. Pfeiffer, and K. West, *Optica* **2**, 1 (2015).
- [7] O. Cotlet, F. Pientka, R. Schmidt, G. Zarand, E. Demler, and A. Imamoglu, arXiv:1803.08509 (2018).
- [8] M. Sidler, P. Back, O. Cotlet, A. Srivastava, T. Fink, M. Kroner, E. Demler, and A. Imamoglu, *Nature Physics* **13**, 255 (2017).
- [9] V. E. Hartwell and D. W. Snoke, *Phys. Rev. B* **82**, 075307 (2010).
- [10] O. L. Berman, R. Y. Kezerashvili, and Y. E. Lozovik, *Phys. Rev. B* **82**, 125307 (2010).
- [11] O. L. Berman, R. Y. Kezerashvili, and Y. E. Lozovik, *Physics Letters A* **374**, 3681 (2010).
- [12] O. L. Berman, R. Y. Kezerashvili, and G. V. Kolmakov, *ACS Nano* **8**, 10437 (2014).
- [13] G. Liu, D. W. Snoke, A. Daley, L. N. Pfeiffer, and K. West, *Proceedings of the National Academy of Sciences* **112**, 2676 (2015).
- [14] D. M. Myers, J. K. Wuenschell, B. Ozden, J. Beaumariage, D. W. Snoke, L. Pfeiffer, and K. West, *Applied Physics Letters* **110**, 211104 (2017).
- [15] Y. Sun, Y. Yoon, M. Steger, G. Liu, L. N. Pfeiffer, K. West, D. W. Snoke, and K. A. Nelson, *Nature Physics* **13**, 870 (2017).
- [16] B. Ozden, D. M. Myers, M. Steger, K. West, L. Pfeiffer, and D. W. Snoke, in *Physics and Simulation of Optoelectronic Devices XXVI*, Vol. 10526 (International Society for Optics and Photonics, 2018) p. 105260H.
- [17] D. M. Myers, B. Ozden, M. Steger, E. Sedov, A. Kavokin, K. West, L. N. Pfeiffer, and D. W. Snoke, *Phys. Rev. B* **98**, 045301 (2018).
- [18] A. Griffin, T. Nikuni, and E. Zaremba, *Bose-condensed gases at finite temperatures* (Cambridge University Press, 2009).
- [19] P. B. Blakie, A. Bradley, M. Davis, R. Ballagh, and C. Gardiner, *Advances in Physics* **57**, 363 (2008).

- [20] C. Gardiner, M. Lee, R. Ballagh, M. Davis, and P. Zoller, *Physical review letters* **81**, 5266 (1998).
- [21] C. N. Weiler, T. W. Neely, D. R. Scherer, A. S. Bradley, M. J. Davis, and B. P. Anderson, *Nature* **455**, 948 (2008).
- [22] T. Neely, A. Bradley, E. Samson, S. Rooney, E. M. Wright, K. Law, R. Carretero-González, P. Kevrekidis, M. Davis, and B. P. Anderson, *Physical review letters* **111**, 235301 (2013).
- [23] T. Neely, E. Samson, A. Bradley, M. Davis, and B. P. Anderson, *Physical review letters* **104**, 160401 (2010).
- [24] A. Bradley, C. Gardiner, and M. Davis, *Physical Review A* **77**, 033616 (2008).
- [25] A. Bradley, S. Rooney, and R. McDonald, *Physical Review A* **92**, 033631 (2015).
- [26] R. McDonald and A. Bradley, *Physical Review A* **93**, 063604 (2016).
- [27] S. Rooney, A. Bradley, and P. Blakie, *Physical Review A* **81**, 023630 (2010).
- [28] G. Gauthier, M. T. Reeves, X. Yu, A. S. Bradley, M. A. Baker, T. A. Bell, H. Rubinsztein-Dunlop, M. J. Davis, and T. W. Neely, *Science* **364**, 1264 (2019).
- [29] S. Mukherjee, A. Bradley, and D. Snoke, in preparation.
- [30] S. Mukherjee, D. Myers, R. Lena, B. Ozden, J. Beaumariage, Z. Sun, M. Steger, L. Pfeiffer, K. West, A. Daley, *et al.*, *Physical Review B* **100**, 245304 (2019).

# Pushing Photons with Electrons: Observation of the Polariton Drag Effect - Supplementary Information

D. M. Myers,<sup>\*</sup> Q. Yao, S. Mukherjee,<sup>†</sup> B. Ozden,<sup>‡</sup> J. Beaumariage, and D. W. Snoke

*Department of Physics and Astronomy,  
University of Pittsburgh, Pittsburgh, PA 15260, USA*

L. N. Pfeiffer and K. West

*Department of Electrical Engineering,  
Princeton University, Princeton, NJ 08544, USA*

(Dated: July 8, 2022)

## PUMPING ON THE HIGH-ENERGY END

In the main text, the data shown and discussed was for the specific case of pumping the wire on the low-energy end, with respect to the cavity gradient. In principle, the asymmetry in momentum can be flipped to the opposite direction by pumping on the opposite side. However, the gradient of the cavity photon energy prevents a clean symmetric change of flow direction. Figure S1 shows a summary of the data when pumping on the high-energy end of the wire. In this case, since the polaritons flow downhill away from the pump, the energy gradient of the condensate is greater than in the case of Figure 2 of the main text. In the opposite case, shown in Figure 2 of the main text with flow on a slight uphill away from the pump, the exciton reservoir helps to level the potential by filling the lowest energy end, and the polariton density is naturally higher near the source. This results in a level potential at relatively low densities. In the case of Figures S1(a) and S1(b), however, the reservoir actually makes the potential even less level, and the polaritons must flow all the way to the opposite end in order to form a level potential. The polaritons do clearly flow the  $\approx 175 \mu\text{m}$  to the far end and form a condensate, but there is no single condensate along the majority of the wire.

Figure S1(c) shows the energy and momentum distributions under similar conditions. The flow is generally in the  $-x$ -direction as expected, but there is not a significant peaked population at large non-zero  $k_{\parallel}$ . As shown in Figure S1(d), which gives the momentum of the particles integrated over energy, a small portion of the population between about  $-0.2$  and  $-0.4 \mu\text{m}^{-1}$  responds to applied voltage. This population shifts toward negative momentum with negative voltage and positive momentum with positive voltage, as expected from the more dramatic shifts shown in the main text. This effect is small, but the overall change in polariton flow from positive to negative in-plane momentum when changing the pump location confirms our claim that the overall momentum is largely due to flow from the pump spot.

## CURRENT-VOLTAGE CHARACTERISTICS

The current vs. voltage characteristics are similar to what was observed in the square pillar devices of Ref. ? , and can be seen in Figure S2. All data shown in the three separate

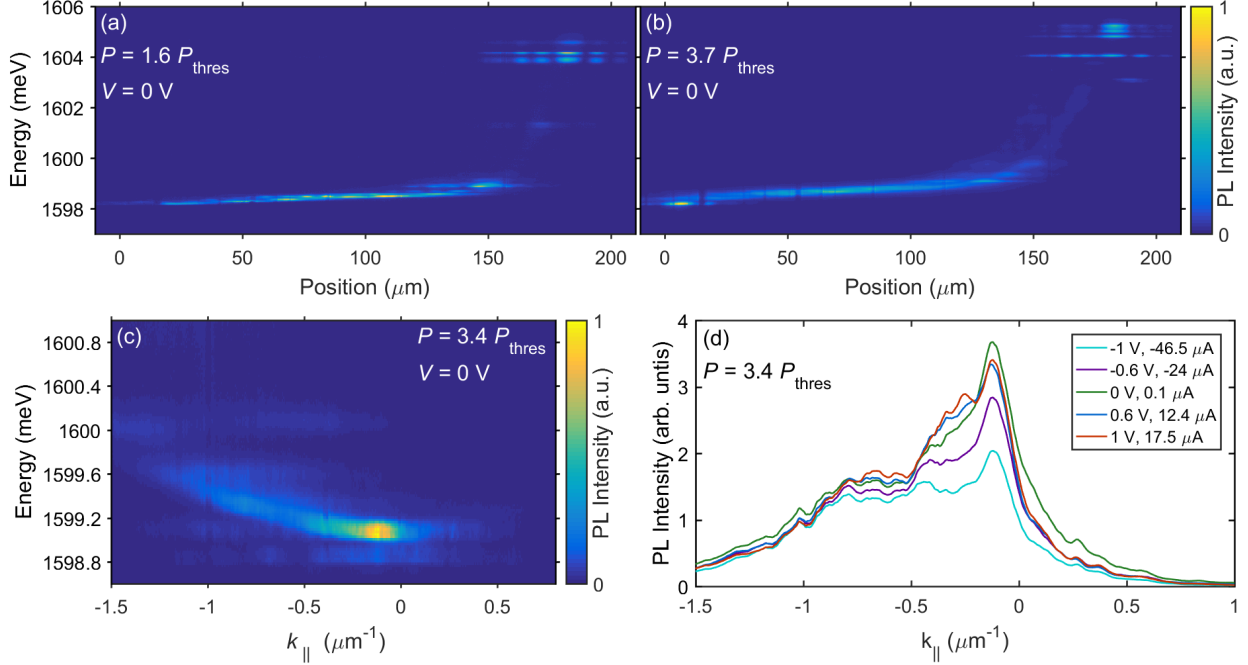


FIG. S1. (a) and (b) show PL intensity of the polaritons vs. energy and position along the length of the wire at zero applied voltage. The threshold power was about 150 mW under these conditions, and the powers used were (a)  $1.6P_{\text{thres}}$  and (b)  $3.7P_{\text{thres}}$ . (c) The PL intensity of the polaritons vs. energy and in-plane momentum ( $k_{\parallel}$ ) zero applied voltage. This image is from a different device from (a) and (b), so the energies are not directly comparable. However, the threshold power was similar, about 150 mW, and the power for the image shown was about  $3.4P_{\text{thres}}$ . (d) PL intensity integrated along the energy axis for data from the same device as (c) and under the same pump conditions.

axes are from the same device and pumped under similar conditions. An overall asymmetry is apparent when pumping on either end of the wire, and especially at lower powers. The asymmetry mostly disappears when pumping in the middle, indicating that it is due to the pump location. Furthermore, the asymmetry is nearly exactly opposite for pumping on opposite ends, which also indicates that it is primarily due to the pump spot location. We attribute this to greater illumination of the contact near the pump spot, creating free carriers that can carry current over the  $n-i$  band bending barrier, as discussed in Ref. ? .

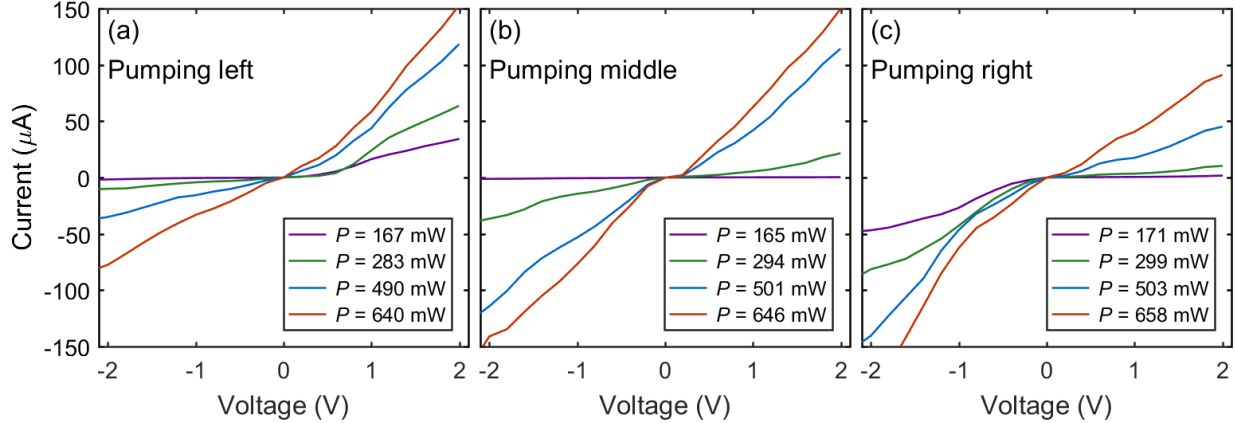


FIG. S2. Current vs. voltage for various pump powers and with different pump spot locations. The locations are given in the upper left of each plot, and are defined in reference to Figure 1(b) of the main text. Specifically, they are the (a) low energy end, (b) middle, and (c) high energy end of the wire, which correspond to the left, middle, and right sides of the  $x$ -axes used throughout this work. The approximate condensate threshold power for each case was (a) 130 mW, (b) 130 mW, and (c) 150 mW.

## NUMERICAL MODEL

In these simulations we obtained a steady state by evolving an initial state  $\psi(x, t = 0)$  under the equations (1) and (3) in the main text. The choice of the initial state only affects the transient dynamics seen in the short time evolution ( $< 500$  ps), but in the long time limit ( $> 4$  ns, much longer than the lifetime of the polaritons  $1/\gamma = 200$  ps) of the evolution, different initial states converge to the same steady state. The CW pump profile is shown in Fig. S3. The effective potential ( $V_\psi(x)$ ) felt by the polaritons due to the cavity gradient in the wire and the repulsive interactions with the excitons at the location of the pump spot is shown in Fig. S4. In a timestep  $dt$  the updated wavefunction  $\psi(x, t + dt)$  is computed in two steps. In the first step, Eqn. 1 is evolved with a fourth-order Runge-Kutta integrator to compute the phase ( $\varphi(x, t + dt)$ ) and density ( $n(x, t + dt) = |\psi(x, t + dt)|^2$ ) of the wavefunction. The norm of the wavefunction is conserved in this step. In the next step, Eqn. 3 is used to calculate the change in the density of the wavefunction  $dn(x, t + dt)$  due to the generation of the polaritons by the pump  $P(x)$ , loss of the polaritons from the cavity  $\gamma$ , and the net flux of the polaritons flowing in the wire  $\nabla \cdot J(x, t)$  using a single step explicit

Euler method. In this step the condensate current  $J(x, t)$  is calculated using the updated wavefunction  $\psi(x, t + dt)$  obtained after the first step. Finally, the updated wavefunction is given by

$$\psi(x, t + dt) = \sqrt{n(x, t + dt) + dn(x, t + dt)} e^{i\varphi(x, t + dt)}. \quad (\text{S1})$$

The drag potential given by Eqn. 2 in the main text is nonlocal in spatial coordinates. Therefore it is efficiently computed in the Fourier space. Assuming the Fourier transform  $\mathcal{F}(\cdot)$  of the scattering matrix  $M(x - x')$  is  $\tilde{M}(q)$ ,  $V_\epsilon(x, t)$  is calculated as

$$V_\epsilon(x, t) = -\mathcal{F}^{-1} \left( \tilde{M}(q) \mathcal{F} \left( \frac{dJ(x, t)}{dx} \right) \right). \quad (\text{S2})$$

The dimensionless scattering matrix used in these simulations is shown in Fig. S5. Fig. 6 in the main text is generated by taking a temporal Fourier transform of the late time real space wavefunction  $\psi(x, t)$  in a  $\sim 300$  ps interval and integrated over 10 such intervals. These plots show the real space spectral density  $|\psi(x, \omega)|^2$  of the condensate. Similarly Fig. 7 is generated by taking a spatial Fourier transform of the late time real space wavefunction  $\psi(x, t)$  and time integrating over  $\sim 3$  ns.

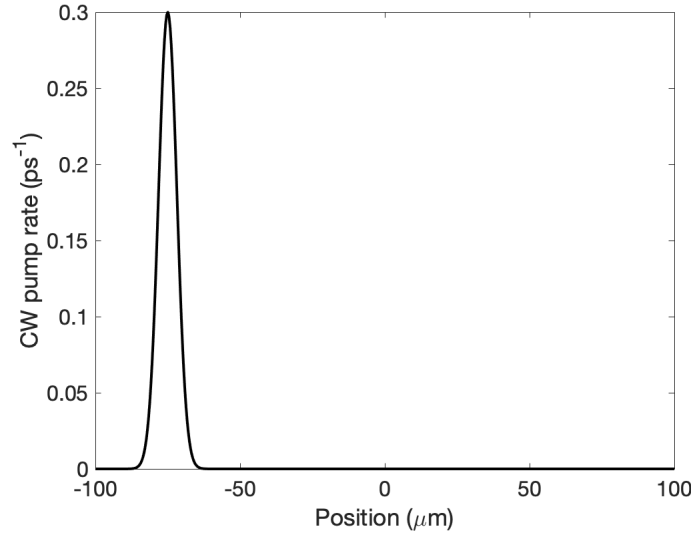


FIG. S3. CW pump profile used in the simulations reported in Fig. 6 and 7 in the main text.

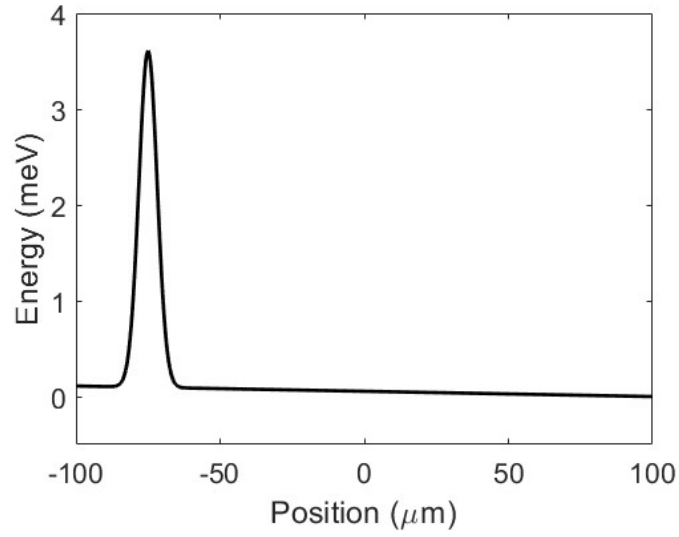


FIG. S4. Effective potential  $V_\psi$  experienced by the polaritons in the wire in the simulations. The ends of the wire are modeled as an open boundary condition.

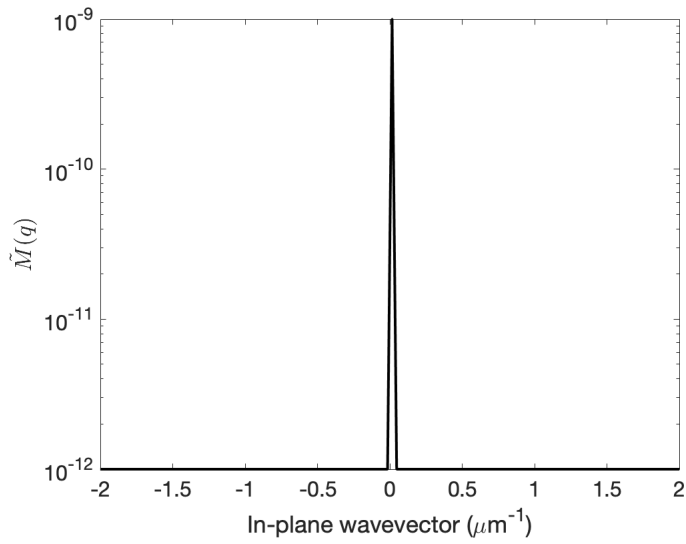


FIG. S5. Dimensionless  $\tilde{M}(q)$  used in the simulations reported in Fig. 6 and 7 in the main text.